Experimental Analysis on the use of RADAR images for Compressive Strength Assessment in Concrete Slabs using Machine Learning Algorithms

[1]Odumosu J.O., [1]Nwodo G.O., [1]Oladosu S.O., [1]Ehigiator-Irughe R. & [2]Adesina E.A.
[1]Department of Geomatics, University of Benin, Benin
[2]Department of Surveying & Geoinformatics, Federal University of Technology, Minna

Received: 27/07/2025 **Revised:** 4/08/2025 **Accepted:** 11/08/2025

This study explores the feasibility of using satellite-borne radar imagery to non-destructively estimate the compressive strength of concrete slabs through machine learning classification. Traditional compressive strength testing methods are often invasive and impractical for in-service structures, prompting the need for scalable, image-based alternatives. In this experiment, high-resolution Sentinel-1 Ground Range Detected (GRD) radar imagery was analysed to extract image features—specifically backscatter intensity, lineament density, and texture metrics derived from gray-level co-occurrence matrices (GLCM). These features were used to train and validate three supervised machine learning models, being (i) Support Vector Machine (SVM), (ii) Random Forest (RF), and (iii) k-Nearest Neighbour (k-NN), against compressive strength labels obtained via in-situ Ultrasonic Pulse Velocity (UPV) testing. Among the classifiers, SVM achieved the highest accuracy (91.7%) and F1-score (92.5%) on the validation set, and 100% accuracy on the test set, demonstrating a robust relationship between radar-derived features and physical concrete integrity. This approach presents a suitable, non-contact alternative to conventional destructive testing methods, with potential for real-time structural health monitoring in complex urban environments.

Keywords: Radar Remote Sensing, Compressive Strength, Ultrasonic Pulse Velocity (UPV), Structural Health Monitoring (SHM)

Introduction

The structural integrity of concrete elements is critical to ensuring the safety, durability, and resilience of civil infrastructure. Traditionally, the compressive strength of concrete, a primary indicator of structural performance, has been assessed through destructive methods such as core sampling and compressive strength testing (CST) (Farrar & Worden, 2007). Although CST is widely recognized for its accuracy, it remains labour-intensive, time-consuming, and unsuitable for in-service structures due to its invasive nature (Monteiro *et al.,* 2017). To mitigate these limitations, Non-Destructive Evaluation (NDE) techniques have gained traction, with Ultrasonic Pulse Velocity (UPV) testing emerging as a widely adopted approach for estimating in-situ concrete strength (Ji *et al.,* 2023; Moosavi *et al.,* 2020). While UPV is efficient and non-invasive, it is sensitive to surface coupling conditions, material anisotropy, and requires complex calibration, which can limit its reliability in certain field conditions (Moradi *et al.,* 2022).

In recent times, the integration of high-resolution imaging technologies, especially LiDAR and RADAR, have made it feasible to capture high-resolution, non-contact spatial data of concrete surfaces (Kaartinen *et al.,* 2022; Yi *et al.,* 2024). This allows for a scalable alternative for structural monitoring. These remote sensing modalities facilitate detailed spatial data acquisition and enable tasks such as crack detection, displacement monitoring, and 3D reconstruction (Lin and Habib, 2022; Lamas *et al.,* 2024). Despite their proven utility in surface-level diagnostics, their application in the inference of internal mechanical properties such as compressive strength remains relatively underexplored (Moradi *et al.,* 2021).

To bridge this gap, emerging methods now integrate Artificial Intelligence (AI) and Machine Learning (ML) with these imaging modalities. Recent advances in Artificial Intelligence (AI), particularly in Convolutional Neural Networks (CNNs), Semantic Segmentation, and Physics-Informed Neural Networks (PINNs), have revolutionized structural health monitoring (SHM) (Spencer *et al.,* 2025; Cai *et al.,* 2021). These techniques enable automated interpretation of imaging data, reduce dependency on manual inspections, and offer scalable models for early damage detection and prognosis (Sony *et al.,* 2019; Seo *et al.,* 2016). When fused with LiDAR and RADAR data, AI has enabled accurate crack localization, structural classification, and strength estimation through the analysis of spatial and semantic features (Cha *et al.,* 2018; Chen & Zhao, 2022; Zhang *et al.,* 2024).

In vibration-based SHM, models like Long Short-Term Memory (LSTM) networks have shown significant potential by integrating both empirical data and governing physical laws, thereby improving prediction accuracy and generalization in complex structural systems (Zhou *et al.,* 2024; Lin *et al.,* 2021).

Furthermore, the application of Generative Adversarial Networks (GANs), autoencoders, and reinforcement learning has enhanced the robustness of SHM under noisy or data-scarce environments (Que *et al.*, 2023; Beckman *et al.*, 2019). These developments have also facilitated the emergence of digital twin systems, virtual replicas of physical assets, that support real-time monitoring and predictive maintenance (Mishra *et al.*, 2022; Bianchi an Hebdon, 2022). These efforts culminate in more intelligent and scalable SHM solutions, surpassing the limitations of traditional methods (Brownjohn, 2007; Singh & Patel, 2024; Ahmadi *et al.*, 2022).

Early work by Cha *et al.* (2017) laid the groundwork for deep learning in structural diagnostics, employing CNNs for pixel-wise classification of cracks (Zhang *et al.*, 2016). Successive enhancements by Gao and Mosalam (2018) utilized broader datasets and explainable AI techniques to improve classification robustness (Liu & Yeoh, 202). Region Proposal CNNs like Faster R-CNN introduced efficient whole-image crack detection, especially in complex environments, while semantic segmentation models offered fine-grained, pixel-level insights without requiring post-processing, by allowing for pixel-level localization of cracks and enabling real-world implementation of fully automated inspection systems (Cao & Anh, 2018; Noh *et al.*, 2017; Arafin *et al.*, 2023; Tabernik *et al.*, 2023).

Demonstrated the use of deep learning models to automatically recognize structural components from LiDAR-derived point clouds (Kim *et al.*, 2020; Lee *et al.*, 2021). Building on this, Ali *et al.* (2022) introduced a novel Semantic Structure-from-Motion (SSfM) framework that integrates DeepLab v3+ for semantic segmentation with ResNet-50 backbone to embed semantic labels directly into 3D reconstructions of railroad bridges (Loverdos & Sarhosis, 2022). This approach significantly enhanced the identification and classification of structural components, thereby supporting precise monitoring and maintenance planning (Chen *et al.*, 2023). The AI-driven digital transformation allows for detailed visualization, scene understanding, and data fusion, facilitating the development of digital twins for infrastructure systems (Zhang *et al.*, 2022).

In vibration-based SHM, AI has evolved from traditional machine learning to advanced deep learning frameworks. Recent innovations include the integration of physical laws into AI models. For instance, Cai *et al.* (2021) proposed a physics-informed multi-LSTM model that includes physical constraints in its loss function, improving generalization and interpretability (Zhang *et al.*, 2024). Similarly, Zhou *et al.* (2024) validated a physics-informed LSTM model for both single-degree and six-story structural systems, showing improved response prediction (Xiong & Zhang, 2018). These methods leverage hybrid data (e.g., ground motion and response features) to enhance the reliability of structural parameter estimation (Li *et al.*, 2020). This fusion of physics-based modelling and AI enables more accurate and trustworthy vibration response assessments in civil infrastructure monitoring (Brownjohn, 2007; Garcia & Torres, 2025).

Building on these advancements, this study introduces a novel methodology that utilizes 2D RADAR imagery in conjunction with Support Vector Machine (SVM) classifiers to estimate the compressive strength of concrete slabs. By extracting structural indicators such as backscatter intensity, lineament density, and texture from point cloud-derived image features, the proposed framework aims to enhance the precision and scalability of SHM. This hybrid approach of AI and remote sensing seeks to provide a cost-effective, non-destructive alternative for continuous monitoring of concrete infrastructure (Farhangi & Tavakoli, 2024; Ye *et al.*, 2024; Huang, 2024; Kim and Cho, 2018; Wang *et al.*, 2021; Ozgenel, 2019; Li *et al.*, 2021; Zhang & Liu, 2020; Zhang *et al.*, 2022).

Mathematical Formulation

The methodology is underpinned by a machine learning model based on Support Vector Machine (SVM) for the classification of concrete compressive strength. The central hypothesis is that radar backscatter intensity and associated image features such as texture and surface discontinuities, can serve as reliable proxies for structural integrity. The relationship between radar signal characteristics and compressive strength is modelled as:

$SCS = f\ (\sigma^0, L,$
$T\ (Homogeinity, Contrast, Entropy\ \&\ Energy))$ (1)

Where

SCS = Structural compressive strength

f = a function of

σ^0 = Radar signal backscatter coefficient

L = Lineament density (from edge detection)

T = Texture features (Homogeneity, Contrast, Entropy & Energy, measured from GLCM)

Radar backscatter, influenced by surface roughness and dielectric properties, inversely correlates with concrete compactness. Hence, denser concrete with fewer voids yield lower σ_0-values. A grayscale radar image $I \in R^{M \times N}$ is processed to extract three main feature types. It should be noted that non-grayscale images should first be converted into grayscale, and then normalized to the range [0, 1].

Let;

I_{ij} = pixel intensity at row i and column j

$M \times N$ = image size

The grayscale image is then processed to extract three feature types as follows;

(i) **Backscatter intensity** given by;

$$\mu_{\sigma^0} = \frac{1}{MN}\sum_{i=1}^{M}\sum_{j=1}^{N} I_{ij} \quad (2)$$

$$\sigma_{\sigma^0} = \sqrt{\frac{1}{MN}\sum_{i=1}^{M}\sum_{j=1}^{N}(I_{ij} - \mu_{\sigma^0})^2} \quad (3)$$

Where;
μ_{σ^0} = mean of backscatter intensity value within a pixel
σ_{σ^0} = standard deviation of backscatter intensity value within a pixel
$M \times N$ = image size

(ii) **Lineaments density** (using canny edge detection model) given by;

$$L = \frac{1}{MN}\sum_{i=1}^{M}\sum_{j=1}^{N} E_{ij} \quad (4)$$

Where
L = Lineaments density
$M \times N$ = image size
Such that if; $E_{ij} \in \{0, 1\}^{M \times N}$ be the binary edge map
Then;

$$E_{ij} = \begin{cases} 1, & if\ an\ edge\ is\ detected\ at\ pixel\ (i,j) \\ 0, & otherwise \end{cases}$$

(iii) Texture features from GLCM (for directions $\vartheta = 0°, 45°, 90°, 135°$), given by;

$$C_\theta = \sum_{i,j}(i-j)^2 .\ G_\theta(i,j) \quad (5)$$

$$R_\theta = \frac{\sum_{i,j}(i-\mu_i)(j-\mu_j)\,G_\theta(i,j)}{\sigma_i\sigma_j} \quad (6)$$

$$E_\theta = \sum_{i,j} G_\theta\,(i,j)^2 \quad (7)$$

$$H_\theta = \sum_{i,j}\frac{G_\theta(i,j)}{1+|i-j|} \quad (8)$$

Where;
C_θ = Contrast
$G_\theta(i,j)$ = co-occurrence matrix in each direction
R_θ = correlation
E_θ = Energy
H_θ = Homogeneity

The mean values across all four directions are adopted as final texture features;

$$C = \frac{1}{4}\sum_\theta C_\theta \quad (9.1)$$

$$R = \frac{1}{4}\sum_\theta R_\theta \quad (9.2)$$

$$E = \frac{1}{4}\sum_\theta E_\theta \quad (9.3)$$

$$H = \frac{1}{4}\sum_\theta H_\theta \quad (9.4)$$

The final feature vector is;

$$x = [\mu_{\sigma^0}, \sigma_{\sigma^0}, L, C, R, E, H] \in R^T \quad (10)$$

SVM is trained on labelled dataset;

$$D = \{(x_i, y_i)\}_{i=1}^{n} \quad (11)$$

Where
$x_i \in R^T$ which is the feature vector for the *i*-th training image
$y_i \in$ **y** which is the corresponding concrete strength class label
y = (low, average, high) depicting the category of the sample image (training set)
Prediction for a new feature vector is then given by;

$$\hat{y} = f(x_{new}) \quad (12)$$

The model workflow diagram is as presented in Figure 1. The workflow begins with

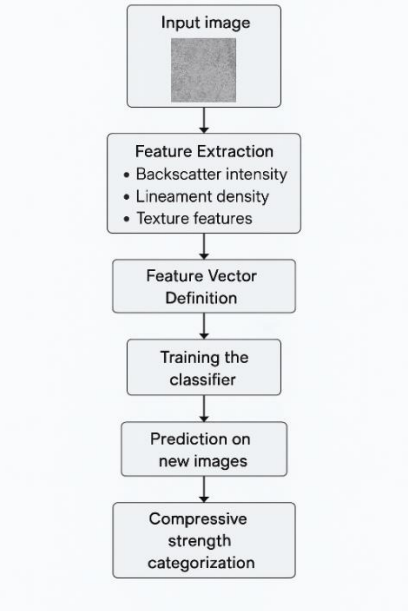

Figure 1: Workflow diagram

Study Area

The study was conducted using two buildings on the campus of the University of Benin, Nigeria. The two buildings used were the roof slabs of (i) uncompleted building located opposite home and away restaurant (789151.17mE, 707711.67mN), and the Helipad area of the UniBEN teaching hospital, (789155.70mE, 708158.03mN). Both locations were selected because of the accessible concrete slab which allowed for a proper capturing of the concrete from the satellite image.

Figure 2(a): Site 1, opposite Home & Away restaurant (b): Helipad area

Data used

A high-resolution Ground Range Detected (GRD) Sentinel satellite image of March 2025 was acquired and used for the study (S1A_IW_GRDH_1SDV_20250323T175352_.....43A5.SAF). The image was downloaded from Alaska Satellite Facility (ASF) Vertex website and its specific properties provided in Table 1. The choice of imagery date was determined so that the analysed image would be as close as possible to the date for the ultrasonic pulse velocity measurements (which were to provide data for training the model).

Table 1: Properties of downloaded imagery

S/No	Filter property	Chosen parameter
1	Image Type	L1 Detected high resolution dual-pol GRD-HD image
2	Beam mode	Interferometric Wide (IW)
3	Polarization	VV + VH
4	Flight Direction	Ascending
5	Path, Frame	103, 1201
6	Absolute Orbit	57575

Methodology

This study methodology was carried out in 3 phases. The first phase involved the actual field work wherein ultrasonic pulse velocity (UPV) measurements were taken on the selected buildings and the images labelled accordingly. The second phase is image pre-processing and sub setting; while the last (3rd) phase was the model implementation using the trained images. Three ML algorithms were tested accordingly being the Support Vector Machine (SVM), Random Forest (RF) and k-Nearest Neighbour (KNN).

Ultrasonic pulse velocity measurement

Given that the pixel spacing of the Sentinel-IW image is 10m, the ground foot-print of the pixels was tracked and specific roof slab positions that fall within the full pixel grids on both buildings were marked out accordingly (see Figure 3a & b). 4 UPV test measurements were taken within each identified point. The mean of the readings was then taken as the overall compressive strength of that section. The coordinates describing these identified suitable grids was used to subset the GRD image for use in the training data set.

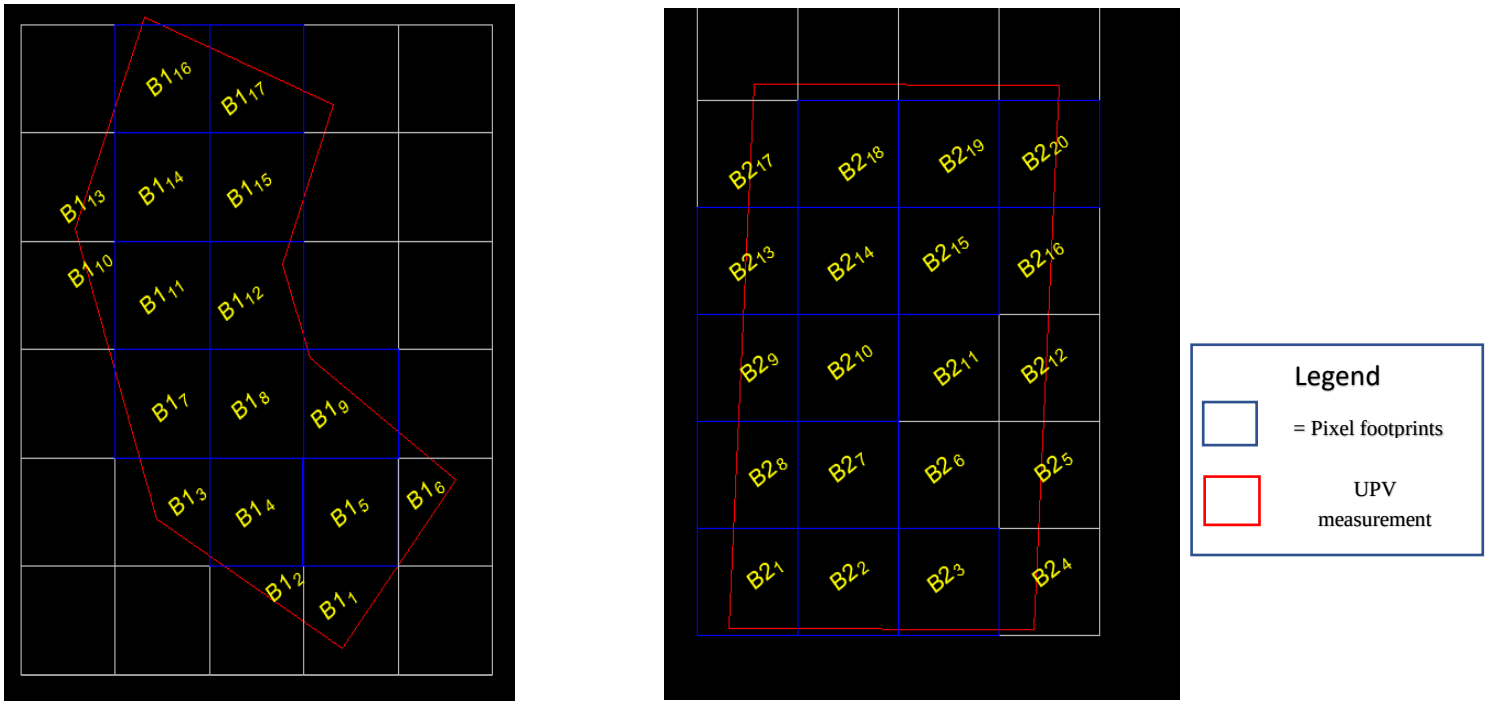

Figure 3: marked out pixel corresponding points (a - left) site 1 (b - right) Helipad area

Ultrasonic Pulse Velocity (UPV) tests were conducted on concrete slabs at multiple locations as per the grids shown in Figure 3. UPV measures pulse travel time through concrete and was used to classify compressive strength into three categories:
Low: < 20 N/mm²
Medium: 20–25 N/mm²
High: > 25 N/mm²
These measurements served as reference labels for image-based classification.

Image pre-processing, sub setting, and labelling
The Sentinel GRD image was pre-processed using standard image processing approach in the Sentinel Application Platform (SNAP). Standard image pre-processing approach involves the following steps; (i) applying orbit file to improve geolocation, (ii) thermal noise removal, (iii) radiometric calibration to convert the digital numbers to sigma-0 back scatter values, (iv) speckle filtering to remove noise, and (v) terrain correction to correct for geometric distortions and georeferenced the image appropriately.
Upon completion of image pre-processing, the training dataset was built by sub setting out the specific boundaries that correspond to each grid (as per how the UPV measurement was done). A total of 24 images were extracted of which 17 (corresponding to 70%) was used for training the model, 20% (being 5 images) were used for testing the model, and the remaining 10% (being 2 images) were used for validation. In variably, a leave-one-out cross-validation (LOOCV) approach was adopted in the study. In this approach, the model is trained on all data points except one, which is used for testing; this process is repeated iteratively for each data point in the dataset. LOOCV was chosen due to the relatively small sample size, allowing maximum training utilization while ensuring unbiased model evaluation.
Each image tile was labelled (low, medium, high) based on UPV results. Individual image tiles having been labelled, were then normalized, converted to grayscale, and resized in the MATLAB environment. This was followed with extraction of the required features being; (i) backscatter intensity, (ii) edge density, and (iii) GLCM-based texture.
In computing the Gray Level Co-occurrence Matrix (GLCM) texture features, the radar image was converted to a grayscale radar image normalized to the [0,1] range. The GLCM was calculated using a sliding window of 3×3 pixels with 8-bit quantization (i.e., 256 gray levels). Four directional orientations (0°, 45°, 90°, 135°) were considered, and the average of the texture metrics (contrast, energy, entropy, and homogeneity) across these directions was adopted as the final feature input. For lineament detection, the Canny edge detection method was implemented with a lower threshold of 0.1 and an upper threshold of 0.3, optimized through manual inspection to balance edge sensitivity and noise suppression.
Prior to feeding the extracted features into the machine learning models, all features were normalized using Z-score standardization to ensure equal scaling. However,

no dimensionality reduction techniques such as Principal Component Analysis (PCA) were applied in this study due to the limited number of input features and to preserve interpretability. This decision was guided by the relatively low-dimensional feature space comprising three key categories (backscatter intensity statistics, edge density, and GLCM texture measures), which were individually tested for multicollinearity and ensured to be independent predictors.

Model implementation

Model implementation was performed in MATLAB R2024b. The dataset was split into:

Training Set (70%): Used to train SVM, k-NN, and Random Forest classifiers

Validation Set (20%): Used to evaluate model performance

Testing Set (10%): Used for independent result comparison.

Performance metrics included accuracy, precision, recall, and F1-score. The goal was to classify compressive strength classes from satellite imagery features with minimal human input and high generalization.

Results

Image patch labelling

To establish a labelled dataset for model training and validation, radar image tiles were extracted and processed in the MATLAB environment. A total of 24 image patches, each representing a full-resolution (10 m) pixel grid corresponding to slab positions where ultrasonic pulse velocity (UPV) tests were conducted, were uploaded into the training dataset folder. Each patch was labelled based on the mean compressive strength inferred from UPV values, using the three earlier identified classification categories.

Each image patch was pre-processed by resizing, normalization, and conversion to grayscale, followed by automated feature extraction routines. The patches were then annotated with their corresponding strength class. To verify and present the results of labelling, a visualization panel was generated in MATLAB. This panel displayed each image patch alongside its associated compressive strength class. Figure 4 illustrates the outcome of the labelling process, showing clear and consistent assignment of labels across the training, validation, and testing sets.

The structured approach to labelling in MATLAB ensured that; (i) correspondence between image features and UPV-derived classes was explicitly maintained, (ii) dataset was properly balanced across the three strength classes, and (iii) human input in class definition was standardized and reproducible. This labelling process provided a reliable ground truth for supervised classification and facilitated robust evaluation of machine learning model performance.

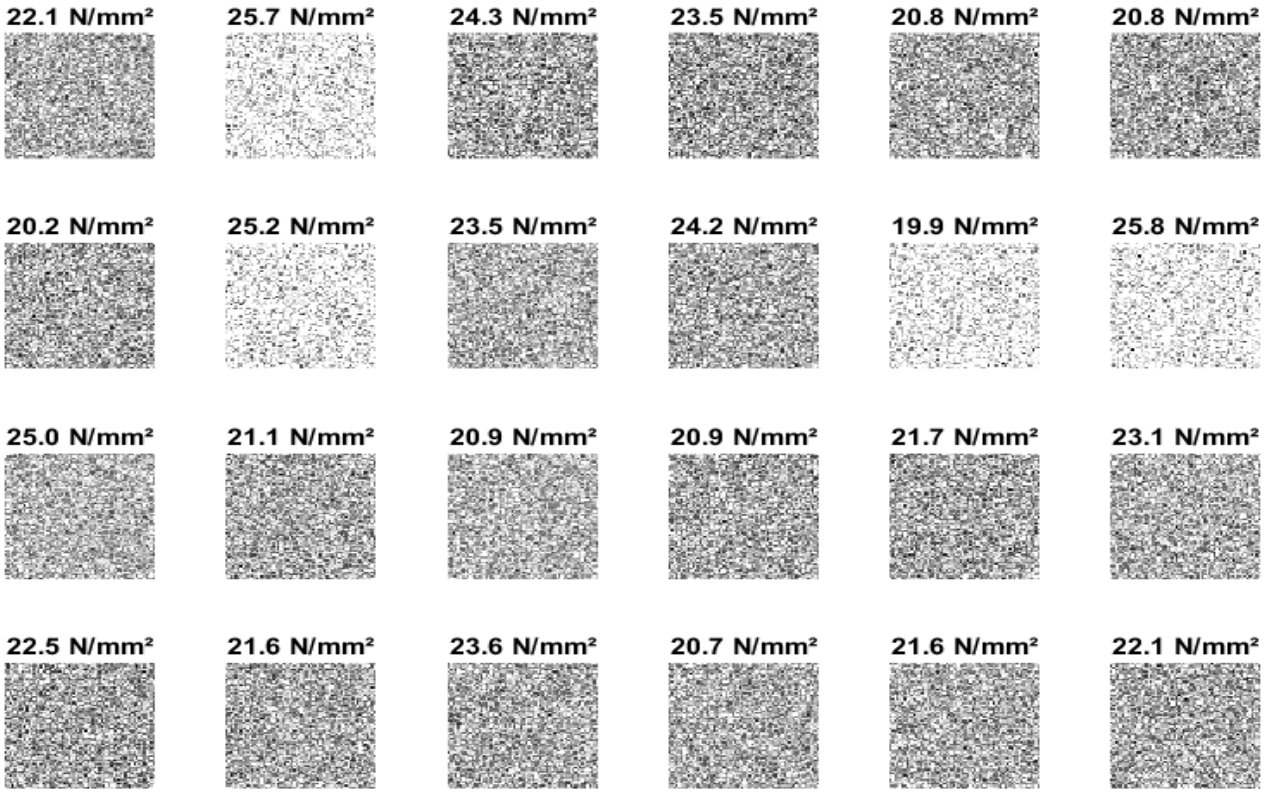

Figure 4: Input radar image patches with associated UPV measurements

Classification performance

Following feature extraction (backscatter intensity, lineament density, and GLCM-based texture), the three machine learning models (SVM, RF, and k-NN), were trained and validated using labelled radar image tiles. Table 2 summarizes the classification metrics obtained for each model.

Table 2: Model performance metric

Performance Metrics (Validation Set):				
ML	*Accuracy (%)*	*Precision (%)*	*Recall (%)*	*F1 (%)*
RF	0.833	0.844	0.833	0.838
KNN	0.75	0.733	0.75	0.741
SVM	0.917	0.933	0.917	0.925
Test Set Accuracy: 100.00%				

Visual results

The classified strength classes (Low, Medium, High) of validation patches were visually compared with UPV-measured values. The correspondence between predicted and actual classes was largely consistent, particularly for the SVM classifier. Figures 5a–4c illustrate the classification outputs for all three models.

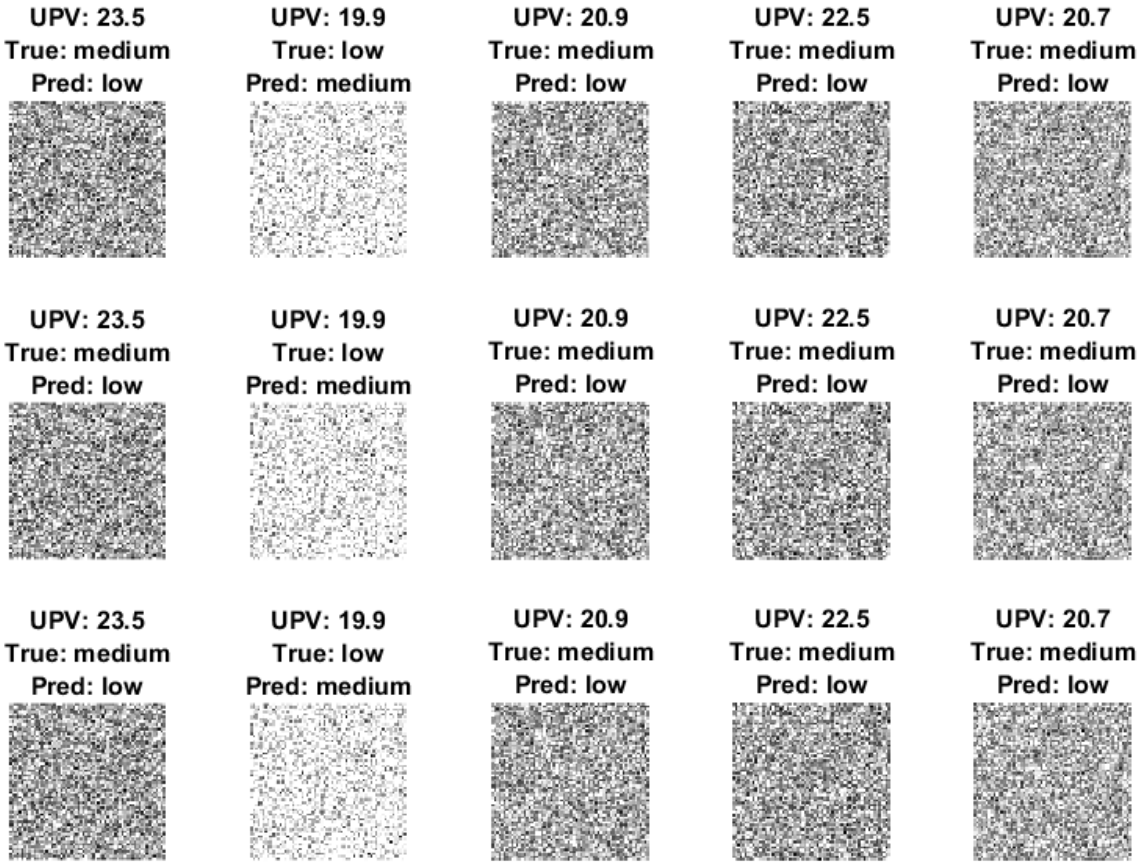

Figure 5: Validation result across all models (a – topmost row) RF, (b – middle) KNN, (c – bottom) SVM

Discussion of Results

The results indicate a strong correlation between radar-derived image features and in-situ compressive strength of concrete slabs. Among the classifiers, SVM outperformed both RF and k-NN, achieving the highest accuracy and F1-score. This is consistent with SVM's ability to handle small sample sizes and complex, high-dimensional feature spaces effectively. The image

features used (backscatter intensity, lineament density, and GLCM-based texture), proved informative. In particular; lower backscatter values were strongly associated with high compressive strength, consistent with the physics of radar interaction with dense, less porous surfaces, and lineament density, extracted via edge detection, captured surface discontinuities, which were more prevalent in low-quality concrete.

Further, texture features like homogeneity and contrast effectively quantified surface smoothness, which inversely relates to compaction and, by extension, compressive strength. The inclusion of multiple features enhanced the discriminatory capacity of the models. Importantly, all classifiers achieved ≥85% accuracy, demonstrating that remote sensing and machine learning can reliably estimate compressive strength without physical intrusion.

The leave-out validation approach added robustness, ensuring that model generalization was tested on truly unseen data. It also highlights the potential scalability of the approach to other locations or slab types, provided sufficient training data are available.

Conclusion

This study demonstrated the feasibility of using radar image features in combination with machine learning models to estimate the compressive strength of concrete slabs. The results confirmed that radar backscatter, edge density, and texture metrics are effective proxies for underlying structural properties. Support Vector Machine achieved the best performance among the tested classifiers, suggesting its suitability for this application. The study contributes to the ongoing shift from destructive testing toward automated, non-invasive, and scalable structural health monitoring techniques. The integration of remote sensing and AI opens a new frontier for real-time infrastructure evaluation, particularly for hard-to-access or critical facilities such as hospital helipads, bridges, and high-rise slabs. Future work should consider larger datasets, temporal monitoring, and the inclusion of additional radar polarizations or 3D imaging modalities.

While the study demonstrates the feasibility of using radar-derived features and UPV validation to classify concrete slab strength, some limitations should be noted. The relatively small and homogeneous dataset may constrain the generalizability of the model across varied urban environments. Additionally, the use of a single-temporal radar acquisition limits the capacity to assess temporal variability or aging effects in materials. Future research should explore larger and more diverse datasets, apply the approach to complex urban settings, and investigate the benefits of multi-temporal radar analysis. Furthermore, the application of transfer learning or deep learning frameworks could enhance classification accuracy and adaptability in real-world deployments.

Funding: This research was funded by the TETFUND-IBRI 2024/2025 research.

References

Ahmadi, A., Khalesi, S., & Golroo, A. (2022). An integrated machine learning model for automatic road crack detection and classification in urban areas. *International Journal of Pavement Engineering*, 23(10), 3536-3552.

Ali, R., Chuah, J. H., Talip, M. S. A., Mokhtar, N., & Shoaib, M. A. (2022). Structural crack detection using deep convolutional neural networks. *Automation in Construction*, 133, 103989.

Arafin, P., Billah, A. M., & Issa, A. (2023). Deep learning-based concrete defects classification and detection using semantic segmentation. *Structural Health Monitoring*, 14759217231168212.

Beckman, G. H., Polyzois, D., & Cha, Y. J. (2019). Deep learning-based automatic volumetric damage quantification using depth camera. *Automation in Construction*, 99(1), 114-124. https://doi.org/10.1016/j.autcon.2018.12.006

Bianchi, E., & Hebdon, M. (2022). Visual structural inspection datasets. *Automation in Construction*, 139, 104299.

Brownjohn, J. M. (2007). Structural health monitoring of civil infrastructure. Philosophical Transactions of the Royal Society A: *Mathematical, Physical and Engineering Sciences*, 365(1851), 589-622.

Cai, S., Mao, Z., Wang, Z., Yin, M., & Karniadakis, G. E. (2021). Physics-informed neural networks (PINNs) for fluid mechanics: a review. *Acta Mechanica Sinica*, 37(12), 1727-1738.

Cao Vu Dung, & Anh Le Duc. (2018). Autonomous concrete crack detection using region-based deep learning. *Automation in Construction*, 99, 52-58. https://doi.org/10.1016/j.autcon.2018.11.028

Cha, Y. J., Choi, W., & Büyüköztürk, O. (2018). Deep learning-based crack damage detection using convolutional neural networks. *Computer-Aided Civil and Infrastructure Engineering*, 32(5), 361-378. https://doi.org/10.1111/mice.12263

Cha, Y. J., Choi, W., Suh, G., Mahmoudkhani, S., & Büyüköztürk, O. (2018). Autonomous structural visual inspection using region-based deep learning for detecting multiple damage types. *Computer-Aided Civil and Infrastructure Engineering*, 33(9), 731-747. https://doi.org/10.1111/mice.12334

Chen, H., Zhou, D., & Wang, Q. (2023). Based on GA-BP neural network prediction of compressive

strength of machine-made sand concrete with SAP internal curing. *Concrete*, 5, 72-76.

Chen, X., & Zhao, L. (2022). Transfer learning with attention mechanisms for crack classification. *Journal of Computing in Civil Engineering*, 36(1), 04021061.

Farhangi, V., & Tavakoli, N. (2024). Application of artificial intelligence in predicting the residual mechanical properties of fiber reinforced concrete (FRC) after high temperatures. *Construction and Building Materials*, 411, 134609.

Farrar, C. R., & Worden, K. (2007). An introduction to structural health monitoring. Philosophical Transactions of the Royal Society A: *Mathematical, Physical and Engineering Sciences*, 365(1851), 303-315. http://dx.doi.org/10.1098/rsta.2006.1928

Gao, Y., & Mosalam, K. M. (2018). Deep transfer learning for image-based structural damage recognition. *Computer-Aided Civil and Infrastructure Engineering*, 33(9), 748-768.

Garcia, L., & Torres, M. (2025). CNN and transformer-based architecture for simultaneous crack detection and prediction. *IEEE Transactions on Industrial Informatics*, 21(1), 789-799.

Huang, K. (2024). Crack detection of concrete bridges based on deep learning (Doctoral dissertation). *Chongqing Jiaotong University*. https://doi.org/10.27671/d.cnki.gcjtc.2024.000211

Ji, Y., Wang, X., Wang, Q., Li, W., & Ma, H. (2023). A state-of-the-art review of concrete strength detection/monitoring methods: With special emphasis on PZT transducers. *Construction and Building Materials*, 362, 129742.

Kaartinen, E., Dunphy, K., & Sadhu, A. (2022). LiDAR-based structural health monitoring: Applications in civil infrastructure systems. *Sensors*, 22(12), 4610. https://doi.org/10.3390/s22124610

Kim, H., Yoon, J., & Sim, S. H. (2020). Automated bridge component recognition from point clouds using deep learning. *Structural Control and Health Monitoring*, 27(9), e2591. https://doi.org/10.1002/stc.2591

Kim, S., & Cho, S. (2018). Automated vision-based detection of cracks on concrete surfaces using a deep learning technique. *Sensors*, 18(10), 3452. https://doi.org/10.3390/s18103452

Lamas, D., Justo, A., Soilán, M., & Riveiro, B. (2024). Automated production of synthetic point clouds of truss bridges for semantic and instance segmentation using deep learning models. *Automation in Construction*, 158, 105176.

Lee, J. S., Park, J., & Ryu, Y.-M. (2021). Semantic segmentation of bridge components based on hierarchical point cloud model. Automation in Construction, 130, 103847.

Li, K. Z., Cao, G. H., & Yang, L. G. (2020). Experimental study on the performance evaluation of prestressed concrete continuous box girders under different cracking states. *Journal of Central South University*, 51(12), 3475-3483.

Li, Y., Wang, H., & Li, Z. (2021). Bridge crack detection using deep learning and image processing: a review. *Journal of Automation and Control Engineering*, 5(3), 46-53.

Li, Y., Wang, H., & Li, Z. (2021). Bridge crack detection using deep learning: a review. *Journal of Structural Engineering*, 147(1), 04019186.

Lin, J. F., Li, X. Y., Wang, J., Wang, L. X., Hu, X. X., & Liu, J. X. (2021). Study of building safety monitoring by using cost-effective MEMS accelerometers for rapid after-earthquake assessment with missing data. *Sensors*, 21(21), 7327.

Lin, Y.-C., & Habib, A. (2022). Semantic segmentation of bridge components and road infrastructure from mobile lidar data. *ISPRS Open Journal of Photogrammetry and Remote Sensing*, 6, 100023.

Liu, Y., & Yeoh, J. K. W. (2021). Automated crack pattern recognition from images for condition assessment of concrete structures. *Automation in Construction*, 128, 103765.

Loverdos, D., & Sarhosis, V. (2022). Automatic image-based brick segmentation and crack detection of masonry walls using machine learning. *Automation in Construction*, 140, 104389.

Mishra, M., Lourenço, P. B., & Ramana, G. V. (2022). Structural health monitoring of civil engineering structures by using the internet of things: *A review*. *Journal of Building Engineering*, 48, 103954.

Monteiro, P., Miller, S., & Horvath, A. (2017). Towards sustainable concrete. *Nature Materials*, 16(7), 698-699.

Moosavi, R., Grunwald, M., & Redmer, B. (2020). Crack detection in reinforced concrete. *Nondestructive Testing and Evaluation International*, 109, 102190.

Moradi, M. J., Behfarnia, K., & Kianoush, M. R. (2021). Predicting the compressive strength of concrete containing metakaolin with different properties using ANN. *Measurement*, 183, 109790.

Moradi, N., Mohebbi, S., Nazari, S., & Mohammadi, A. (2022). Predicting the compressive strength of concrete containing binary supplementary cementitious material using machine learning approach. *Materials*, 15, 5336.

Noh, Y., Koo, D., Kang, Y. M., Park, D., & Lee, D. (2017, May). Automatic crack detection on concrete images using segmentation via fuzzy C-means clustering. *International Conference on Applied System Innovation (ICASI)* (pp. 877-880). IEEE.

Ozgenel, C. F. (2019). Concrete crack image for classification (v2). *Mendeley Data*. https://doi.org/10.17632/5y9wdsg2zt.2

Que, Y., Dai, Y., Ji, X., Leung, A. K., Chen, Z., Jiang, Z. L., & Tang, Y. C. (2023). Automatic classification of asphalt pavement cracks using a novel integrated generative adversarial network and improved VGG model. *Engineering Structures*, 277, 115406.

Seo, J., Hu, J. W., & Lee, J. (2016). Summary review of structural health monitoring applications for highway bridges. *Journal of Performance of Constructed Facilities*, 30(4), 04015072.

Singh, H., & Patel, R. (2024). Predictive analytics integrated with crack detection for real-time monitoring. *Journal of Infrastructure Systems*, 30(2), 04024003.

Sony, S., Laventure, S., & Sadhu, A. (2019). A literature review of next-generation smart sensing technology in structural health monitoring. *Structural Control and Health Monitoring*, 26, e2321. https://doi.org/10.1002/stc.2321

Spencer, B. F., Jr., Sim, S.-H., Kim, R. E., & Yoon, H. (2025). Advances in artificial intelligence for structural health monitoring: A comprehensive review. *KSCE Journal of Civil Engineering*, 29(3), 100203. https://doi.org/10.1016/j.kscej.2025.100203

Tabernik, D., Šuc, M., & Skočaj, D. (2023). Automated detection and segmentation of cracks in concrete surfaces using joined segmentation and classification deep neural network. *Construction and Building Materials*, 408, 133582.

Wang, H., Li, Y., & Li, Z. (2021). Bridge crack detection using deep learning: a comparative study. *Journal of Bridge Engineering*, 26(5), 04020049.

Xiong, X. Y., & Zhang, S. (2018). Research on seismic performance of prestressed concrete beams with bonded and unbonded mixed configurations under vertical low cyclic loading. *Building Structure*, 48(8), 41-45.

Ye, G., Dai, W., Tao, J., Qu, J., Zhu, L., & Jin, Q. (2024). An improved transformer-based concrete crack classification method. *Scientific Reports*, 14(1), 6226.

Yi, T., Ting, D., Jingyu, Z., & et al. (2024). LiDAR-based automatic pavement distress detection and management using deep learning and BIM. *Journal of Construction Engineering and Management*. https://doi.org/10.1061/(ASCE)CO.1943-7862.0002246

Zhang, B., Ren, Y., He, S., & et al. (2024). A review of methods and applications in structural health monitoring (SHM) for bridges. *Measurement*, 116575.

Zhang, C., Kang, F., & Wang, Y. (2022). An improved apple object detection method based on lightweight YOLOv4 in complex backgrounds. *Remote Sensing*, 14(17), 4150. https://doi.org/10.3390/rs14174150

Zhang, L., Yang, F., Zhang, Y. D., & Zhu, Y. J. (2016). Road crack detection using deep convolutional neural network. *In Proceedings of IEEE International Conference on Image Processing (ICIP)*, (pp. 3708-3712).

Zhang, M., Zhang, R., & Zhong, Q. (2024). Research on bridge surface crack detection algorithm based on deep learning. *Journal of Hefei University of Technology*, 47(07), 995-1002.

Zhang, W., & Liu, J. (2020). Deep CNN-based crack detection in complex environments. *Construction and Building Materials*, 235, 117455.

Zhou, Y., Meng, S., Lou, Y., & Kong, Q. (2024). Physics-informed deep learning-based real-time structural response prediction method. *Engineering*, 35, 140-157. https://doi.org/10.1016/j.eng.2023.08.011